Infrared Physics and Technology 91 (2018) 243–249

Contents lists available at ScienceDirect

Infrared Physics & Technology

journal homepage: www.elsevier.com/locate/infrared

Regular article

Infrared fix pattern noise reduction method based on Shearlet Transform

Shenghui Rong, Huixin Zhou*, Dong Zhao, Kuanhong Cheng, Kun Qian, Hanlin Qin

School of Physics and Optoelectronic Engineering, Xidian University, Xi'an, Shaanxi 710071, China

ARTICLE INFO

Keywords:
Infrared focal plane array
Non-uniformity correction
Temporal high-pass filter
Shearlet transform

ABSTRACT

The non-uniformity correction (NUC) is an effective way to reduce fix pattern noise (FPN) and improve infrared image quality. The temporal high-pass NUC method is a kind of practical NUC method because of its simple implementation. However, traditional temporal high-pass NUC methods rely deeply on the scene motion and suffer image ghosting and blurring. Thus, this paper proposes an improved NUC method based on Shearlet Transform (ST). First, the raw infrared image is decomposed into multiscale and multi-orientation subbands by ST and the FPN component mainly exists in some certain high-frequency subbands. Then, high-frequency subbands are processed by the temporal filter to extract the FPN due to its low-frequency characteristics. Besides, each subband has a confidence parameter to determine the degree of FPN, which is estimated by the variance of subbands adaptively. At last, the process of NUC is achieved by subtracting the estimated FPN component from the original subbands and the corrected infrared image can be obtained by the inverse ST. The performance of the proposed method is evaluated with real and synthetic infrared image sequences thoroughly. Experimental results indicate that the proposed method can reduce heavily FPN with less roughness and RMSE.

1. Introduction

The non-uniformity of infrared focal plane array (IRFPA) seriously degrades the imaging quality of infrared system, which will impose a fix pattern noise (FPN) on the image. This phenomenon is mainly caused by response characteristics of the material and read-out circuit of IRFPA. Compared to manufacturing improvement, the non-uniformity correction (NUC) is an efficient and economical way to achieve high-quality infrared images.

A direct way of NUC is to calibrate the response of each detector unit based on a uniform radiation source, which is categorized as reference-based NUC (RBNUC). Two-point [1] and multi-point [2] calibration methods can be utilized to calculate the correction parameters. Though the principle is simple, repeated correction process is needed due to the temporal drift of response characteristic, which will decline the reliability of the imaging system.

Others NUC methods correct FPN by the statistic characteristic of the scene that can be categorized as scene-based NUC (SBNUC). Compared with RBNUC, SBNUC methods only depend on the information of imaging scene, which will reduce the operational complexity and avoid imaging interruption. For instance, the constant statistics base NUC (CS-NUC) methods assume that the first and second order statistics of each detector output should be the same over a sufficient time [3,4]. Neural network based NUC (NN-NUC) methods utilize a least mean square method to adaptively determine the correction parameters based on a desired value [5]. The registration-based NUC (RG-NUC) methods assume that outputs of different detectors are identical under the same irradiance between the frames and the true scene values can be achieved by averaging the registered pixels [6]. The temporal high-pass filtering based NUC (THP-NUC) methods remove the FPN due to its low-frequency characteristic in temporal domain.

Though the implementation of the SBNUC method is much more convenient than the RBNUC method, most of SBNUC methods suffer from the image blurring and ghosting. The reason is the inaccurate estimation of the correction parameters under the static and dynamic situation, respectively. Generally, if a portion of the image temporarily keep static, it is difficult to distinguish the static object and the unchanging FPN. The static object may be suppressed as the FPN and the image blurring would occur. After the motion resumes, the NUC method cannot adjust correction parameters immediately and the ghosting would occur because of these wrong correction parameters.

In order to overcome these drawbacks, various improved methods have been proposed. Zhou et al. [7] combined the temporal and spatial correlation to constrain the assumption of CS-NUC. In NN-NUC methods, more accurate initial estimation and adaptive parameters update rate are two important strategies. Vera et al. [8] proposed an adaptive update rate of correction parameters based on anisotropic total variation method. Yu et al. [9] set two different update rates for the gain and offset parameters respectively, which is more accurate and robust. Rong et al. [10] utilized the guided image filter to estimate the

* Corresponding author.
E-mail address: hxzhou@mail.xidian.edu.cn (H. Zhou).

https://doi.org/10.1016/j.infrared.2018.05.002
Received 9 January 2018; Received in revised form 2 May 2018; Accepted 2 May 2018
Available online 05 May 2018
1350-4495/

desired initial image. The performance of RG-NUC methods is sensitive to the accuracy of registration between adjacent frames, especially under the rotation and affine transformation. Zhuang and Wang [11] introduces the speeded up robust features extraction (SURF) method to handle the deformation between adjacent frames. Rong et al. [12] divided the image into many small patches to generate a set of motion vectors, which can be used to describe the motion accurately. Besides, Maggioni et al. [13] constructed a 3D image volume firstly, then transform this volume into DC (direct current) coefficients and FPN can be removed by a spatiotemporal filter at last. Pipa et al. [14] used recursive least-square and affine projection techniques that jointly compensate for both the bias and gain component of each image pixel.

Although traditional THP-NUC methods overly dependent on the motion of the scene, it is still a promising method. Qian et al. [15] separated the raw image by a spatial low-pass filter and only use the spatial high-frequency component part of image to estimate the FPN. Zuo et al. [16] utilized the bilateral filter to obtain a more accurate FPN separation. Li et al. [17] set different update rate based on the motion and brightness variance between the adjacent frames.

However, these measures are not sufficient to recover the image, especially under the serious FPN. Besides, the column or row of the IRFPA usually shares the same read-out circuit, thus the FPN usually appears striped pattern. Commonly used image decomposition methods are difficult to eliminate striped noise. Thus, in this paper, an improved method is proposed based on the Shearlet Transform (ST). First, the image is decomposed into multiscale subbands by Laplacian Pyramid and then a set of shear filters is utilized to decompose the scaled images into multi-orientation subbands. During this process, different information of the original image are separated into different subbands. Based on the variance of each subbands, a FPN confidence parameter of temporal filter is calculated to eliminate the FPN adaptively. At last, the corrected image is achieved by the inverse ST.

The remainder is organized as follow. In Section 2, the basic principle of THP-NUC are introduced. In Section 3, the proposed method based on multiscale system of Shearlet is discussed in detail. In Section 4, real and synthetic infrared sequences are utilized to verify the performance of the proposed method and the conclusion is given in Section 5.

2. Related work

2.1. Infrared sensor response model

The response of each detection-element in an IRFPA can be approximated as a linear model, which is defined as

$$x^t(m, n) = g^t(m, n) \times y^t(m, n) + f^t(m, n) \tag{1}$$

where t indicates frame index, (m, n) is the pixel location, x is the observed data form the infrared sensor, y is the ideal infrared radiation of the scene, f and g are the offset and gain component of non-uniformity respectively. Generally, the influence of gain component is relatively smaller, which can be approximated as 1 in practical application. The aim of the NUC is to recovery y form x, which can be expressed as follows (for the simplicity, the pixel location is omitted)

$$\hat{y}^t = x^t - f^t \tag{2}$$

where $\hat{y}^t$ is the corrected infrared image.

2.2. THP based non-uniformity correction

The THP-NUC methods assume that the FPN changes very slowly than the scene over time, which means the temporal high-frequency information belongs to the scene and temporal low-frequency information belongs to FPN. In this way, a temporal filter can be utilized to estimate the FPN as

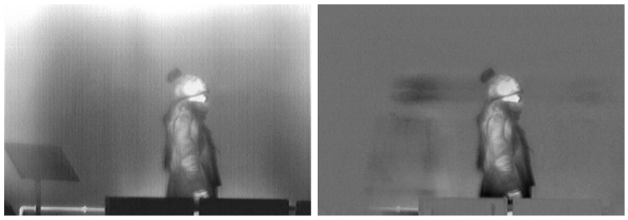

Fig. 1. The drawback of THP-NUC. (a) raw image (b) correction result.

$$f^t = \frac{1}{M} \bullet x^t + \left(1 - \frac{1}{M}\right) \bullet f^{t-1} \tag{3}$$

where M is time constant which can adjust the filter characteristic. This method is strict to the motion of the scene, which will always lead to some unappealing outcomes. Firstly, if a target remains stationary for a relatively long time, it will be filtered out as FPN. Secondly, if an object is moving from static status, a ghosting will appear on corrected frame and fade gradually. This is mainly because the THP-NUC is a kind of recursive process and its output is not only related to the input but also related to the previous correction result. If there is a large error on the estimated FPN, this error will seriously affect the subsequent correction result. An example of THP-NUC result is shown in Fig. 1. This sequence is captured with a static camera, which consists of a stationary background and a moving person. As can be seen from the correction result, although the stripe FPN is completely removed, only the moving person is clearly preserved. The static object at the bottom left of the image is considered as FPN and filtered. Besides, in the opposite direction of the moving person, a large area of ghost is left.

In order to overcome this shortcoming, it is reasonable to decompose the input image as detail component and contour component. This is because the FPN usual acts as spatial high-frequency component, such as point and stripe pattern. If the FPN is estimated only by the high-frequency component, most of scene can be remained and the ghosting can be suppressed. This process can be expressed as

$$x^t = x_H^t + x_L^t \tag{4}$$

$$f^t = \frac{1}{M} \bullet x_H^t + \left(1 - \frac{1}{M}\right) \bullet f^{t-1} \tag{5}$$

where H and L indicate the high and low spatial frequency components, respectively. In this way, the static scene can be retained as much as possible. The whole process of this THP-NUC is illustrated in Fig. 2.

3. The improved THP-NUC method

As described in Section 2, the main problem of the THP-NUC is how to decompose the raw infrared image accurately. The Shearlet Transform (ST) is a useful mathematical tool which can decompose the image into a set of subbands. The FPN mainly exists in certain subbands because of its unique direction. In this section, we first introduce the main principle of ST. Then, we propose an FPN confidence parameter based on the variance of each subbands to control the temporal filter degree. At last, the whole process of proposed method is summarized.

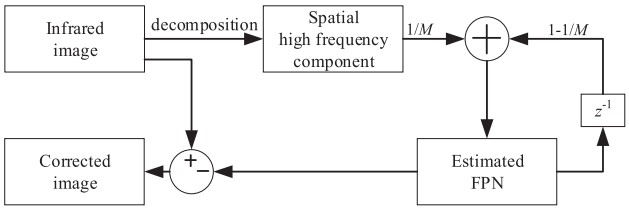

Fig. 2. The flow chart of typical THP-NUC method.

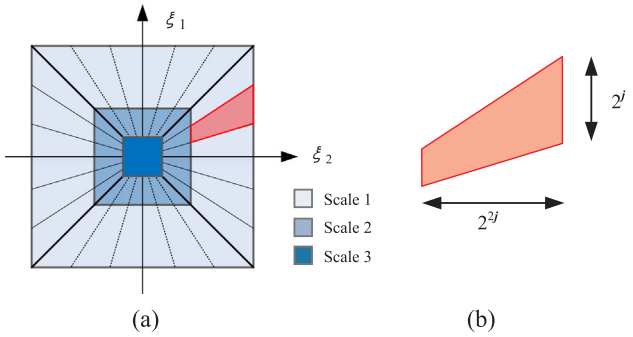

Fig. 3. Frequency plane and support (a) the tiling of frequency by the shearlet (b) the size of the frequency of a shearlet (trapezoid of size $2^{2j} \times 2^{j}$).

3.1. Shearlet base image decomposition

The Shearlet Transform is an extension of the wavelet in case that combines the multiscale and multi-orientation analysis, separately [18]. A Shearlet Transform $\mathscr{SH}_{\psi}$can maps the image $\boldsymbol{I} \in L^2(\Re^2)$to a set of coefficients $\boldsymbol{I}_{j,k,m}$associated with the scale index j, the orientation index k and the position index m, which is defined as

$$\boldsymbol{I}_{j,k,\mathrm{m}} = \mathscr{SH}_{\psi}(\boldsymbol{I}),\ (j,\ k,\ m) \in \mathbb{Z} \times \mathbb{Z} \times \mathbb{Z}^2 \tag{6}$$

where the function $\psi \in L^2(\mathbb{R}^2)$ is known as the mother shearlet defined as

$$\psi_{j,k,m}(x) = 2^{\frac{3}{4}j}\psi(A_{2^j}S_k x - m),\ (j,\ k,\ m) \in \mathbb{Z} \times \mathbb{Z} \times \mathbb{Z}^2 \tag{7}$$

where A is a scaling matrix and S a shearing matrix defined respectively by

$$A_a = \begin{pmatrix} a & 0 \\ 0 & \sqrt{a} \end{pmatrix},\ S_s = \begin{pmatrix} 1 & s \\ 0 & 1 \end{pmatrix} \tag{8}$$

where $a \in \Re^+$ and $s \in \Re$. The anisotropic dilation A_a controls the scale of the shearlets by applying a different dilation factor along the two axes. The shearing matrix S_s determines the orientation of the shearlet. Fig. 3 shows the frequency tiling of the cone-adapted shearlet system generated by the classical ST.

Through the ST, an infrared image can be efficiently decomposed into multiscale and multi-orientation subbands. Each subband can carry different information of the original image. Thus, the FPN can be separated from the original image into certain subband. Fig. 4 gives an example of applying a ST (3 scales and 10 orientations) on a FPN corrupted infrared image, yielding a low-frequency subband and a series of high-frequency subbands. As can be seen from the Fig. 4, image approximation information is concentrated in the low-frequency subband, while the high-frequency subbands contain spatial detail information, such as FPN and edge of the person.

After the ST, the FPN and other detail information of the original image are separated into high-frequency subbands and the stripe FPN mainly exists in the 8-th orientation. Thus, during the correction process, only the high-frequency subbands with most FPN are selected and utilized to estimate the FPN, while other subbands remain unchanged. In this way, the image detail can be reserved as much as possible even in the static situation and the drawback of image blurring can be overcome.

At last, the corrected image $\hat{\boldsymbol{I}}$ can be recovered with modified coefficients $\hat{\boldsymbol{I}}_{j,k,m}$ by inverse Shearlet Transform (IST), expressed as

$$\hat{I} = \mathscr{ISH}_{\psi}(\hat{I}_{j,k,m}),\ (j,\ k,\ m) \in \mathbb{Z} \times \mathbb{Z} \times \mathbb{Z}^2 \tag{9}$$

3.2. The FPN confidence parameter

The ST is a more accurate image decomposition method than mean filter and bilateral filter. However, the accuracy of decomposition is

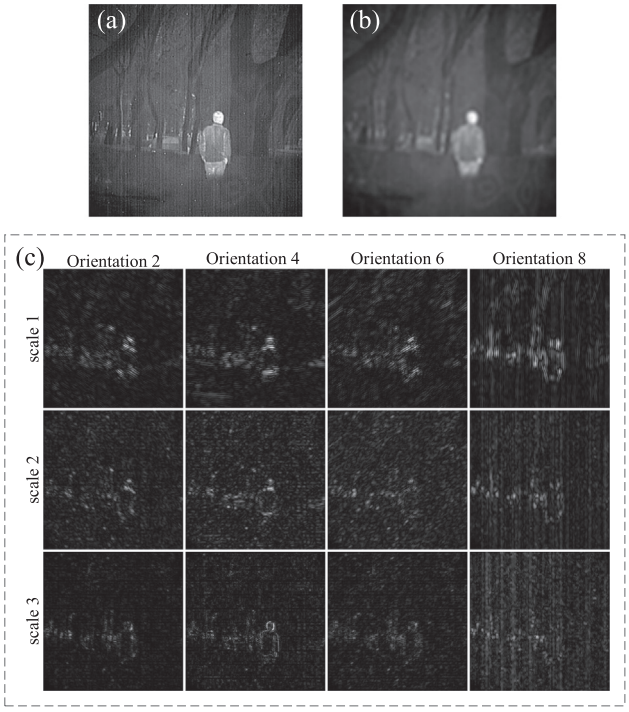

Fig. 4. An illustration of the shearlet transform. (a) original image. (b) the ST low-frequency subband. (c) visualization of the high-frequency ST subbands with 3 scales and selected orientations.

associated with number of scale and the orientation. Generally, the larger number of scales and orientations, the finer the coefficient is. Thus, a larger number of orientation is needed to obtain an accurate decomposition. In this situation, it's difficult to determine which subbands should be selected to estimate the FPN. For instance, the stripe FPN mainly exists in the subband with the vertical information. Due to a larger number of orientations, other subbands with the approximately vertical direction will also carry less degree of the FPN.

Thus, in this paper, a parameter $\alpha \in [0, 1]$ called FPN confidence is proposed and implemented as

$$f_{j,k}^{t} = \alpha_{j,k}^{t} \bullet \left[\frac{1}{M} \bullet x_{j,k}^{t} + \left(1 - \frac{1}{M}\right) \bullet f_{j,k}^{t-1}\right] \tag{10}$$

where $x_{j,k}^{t}$ indicate the subband image at j-th scale and k-th orientation. The correction processed can be expressed as

$$\hat{y}_{j,k}^{t} = x_{j,k}^{t} - f_{j,k}^{t} \tag{11}$$

where $\hat{y}_{j,k}^{t}$ is the estimated non-FPN subband and the final corrected infrared image can be obtained by inverse Shearlet Transform.

In this way, the reduction degree of temporal filter can be adjusted. For the subband with heavy FPN, α should be close to 1. The temporal low-frequency information should be filtered as much as possible. For the subband with light FPN, α should be close to 0 and this component could be remained. In all, different subbands have different filter degree. A more accurate FPN estimation can be achieved and the drawback of ghost can be overcome. In the following, we will discuss how to select this FPN confidence parameter adaptively.

According to the fundamental theory of ST, the high-frequency subband coefficients are modeled as zero-mean and approximately follow the Gaussian distribution, which has been used in many image processing application [19]. The corresponding histograms of shearlet coefficients in Fig. 4 are shown in Fig. 5. Due to the directionality, we assume that the variance of FPN is relatively large in some certain. As shown in Fig. 5, the histogram of the 8-th orientation subband have much flatter shaper than others, which means these subbands have larger variance. This phenomenon is consistent with the visualization of

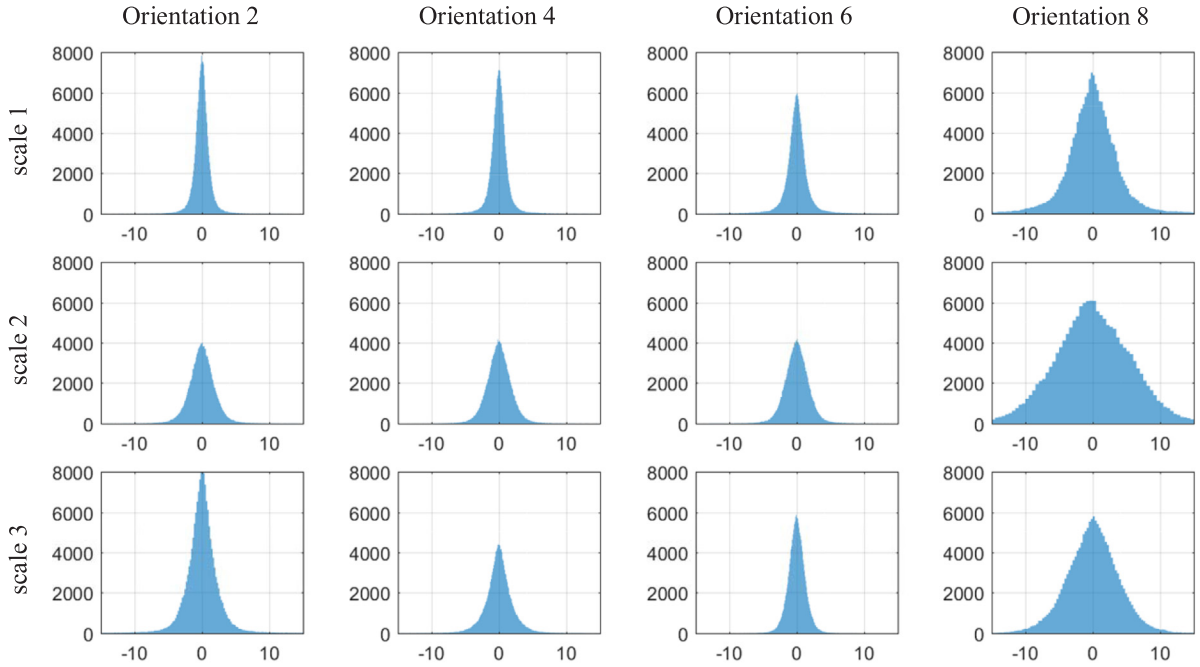

Fig. 5. Histogram of the shearlet coefficients shown in Fig. 4.

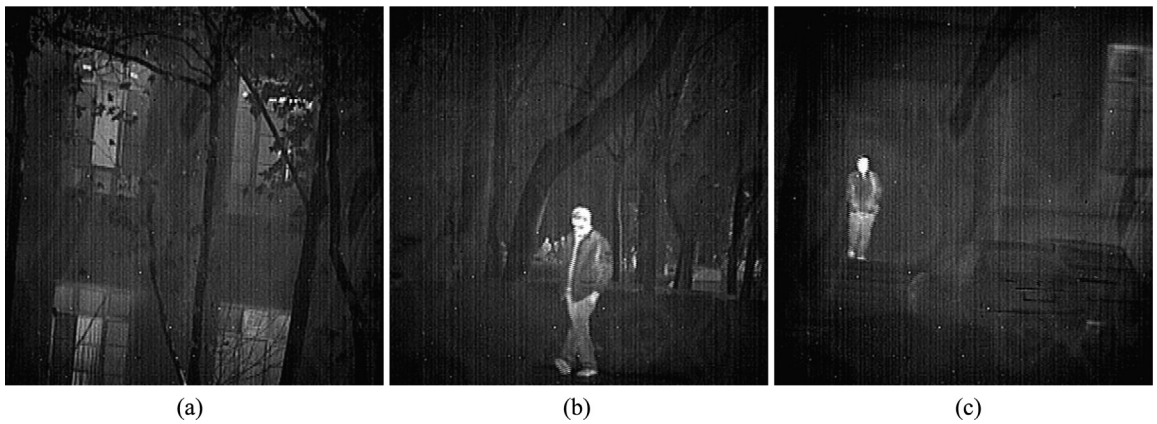

Fig. 6. Raw infrared images. (a) sequence 1 (b) sequence 2 (c) sequence 3.

the corresponding subbands. Thus, the variance of each subband image is an important feature to express the subbands.

Recall the infrared sensor response model $x = y + f$ with y and f independent of each other [20], hence

$$\sigma^2(x_{j,k}^t) = \sigma^2(y_{j,k}^t) + \sigma^2(f_{j,k}^t) \tag{12}$$

where σ^2 is the variance operation. In order to estimate the variance of FPN $\sigma^2(f_{j,k}^t)$, the variance of observation $\sigma^2(x_{j,k}^t)$ and true component $\sigma^2(y_{j,k}^t)$ should be calculated first. The variance of the observation can be calculated directly form the coefficient of subbands. Next, we need to estimate the real signal variance at each subband in a proper way.

Generally, a nature image will contain various content with different directions. Thus, the variance of each subband image is similar and relatively smaller. Based on this assumption, estimate the signal variance can be estimated by averaging all the subbands at the same scale as

$$\hat{\sigma}^2(y_j^t) = \frac{1}{\mathbb{K}} \sum_{k}^{\mathbb{K}} \sigma^2(y_{j,k}^t) \tag{13}$$

where $\mathbb{K}$ indicates the total orientation number of j-th scale shearlet. Then, the variance of the FPN can be estimated as

$$\hat{\sigma}^2(f_{j,k}^t) = \max[\sigma^2(x_{j,k}^t) - \hat{\sigma}^2(y_{j,k}^t), 0] \tag{14}$$

The max operation can avoid the minus and calculate essential FPN. The estimated variance of FPN has the same trend as the FPN confidence parameter. The subband with larger FPN variance should be filtered heavily and the subbands with smaller FPN variance should be filtered lightly. Thus, the estimated variance can be utilized to guide the correction process. Besides, in order to scale the variance into the constant range, a general sigmoid function is introduced as

$$\alpha_{j,k} = \frac{1 - e^{-\varepsilon \cdot \hat{\sigma}^2(f_{j,k}^t)}}{1 + e^{-\varepsilon \cdot \hat{\sigma}^2(f_{j,k}^t)}} \tag{15}$$

where the ε is a shape parameter to adjust the shape of sigmoid function. In this way, the FPN confidence α can be scaled form 0 to 1.

3.3. Summary of the proposed method

In summary, the detail steps of the proposed NUC method are summarized as follows.

Step 1: Initialize correction parameters M and the scale and orientation parameter of ST.

Step 2: implement the ST to the original image x^t and achieve a set

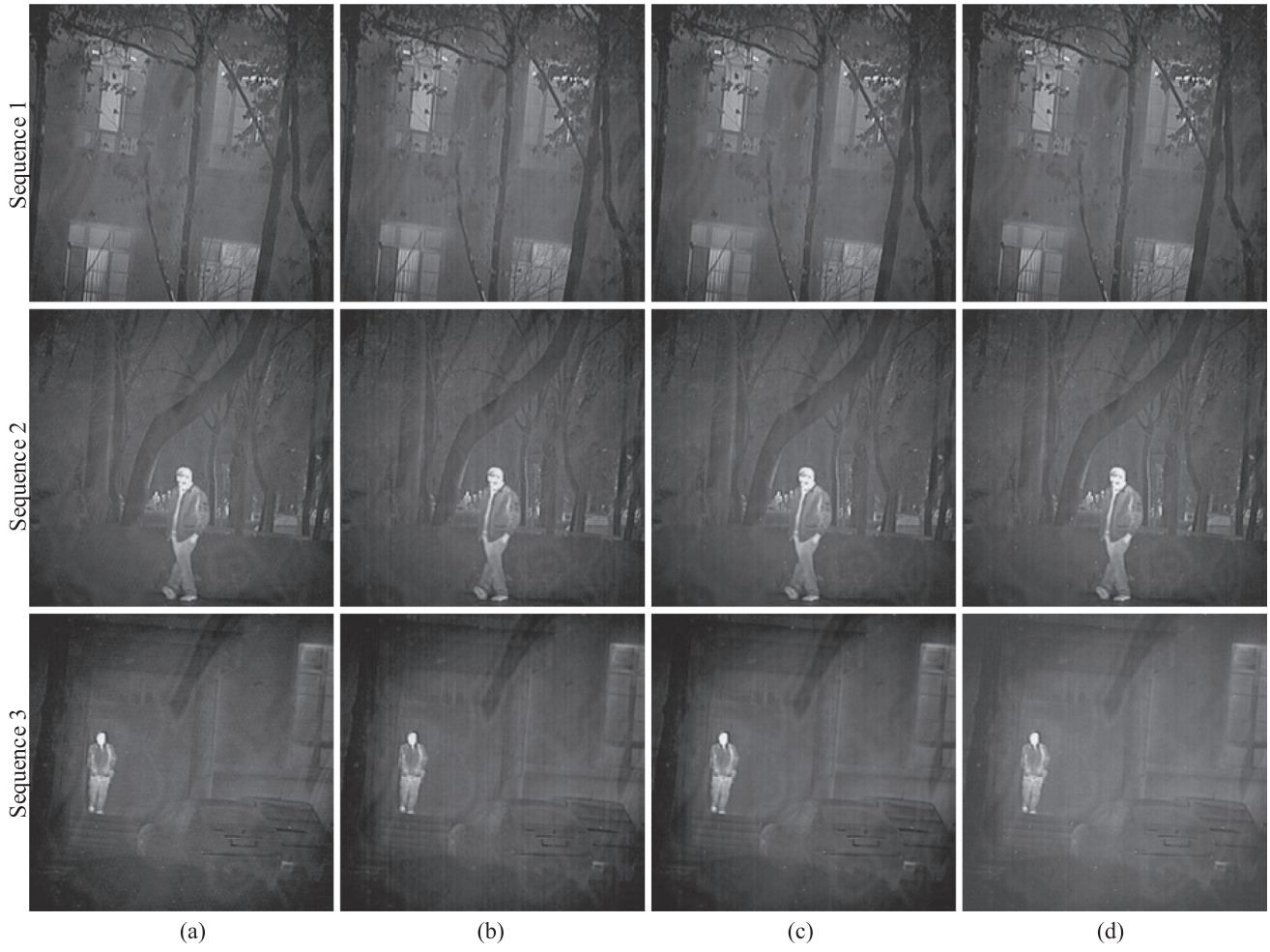

Fig. 7. The correction results. (a) STTH, (b) SLTH, (c) BFTH, (d) MDTH.

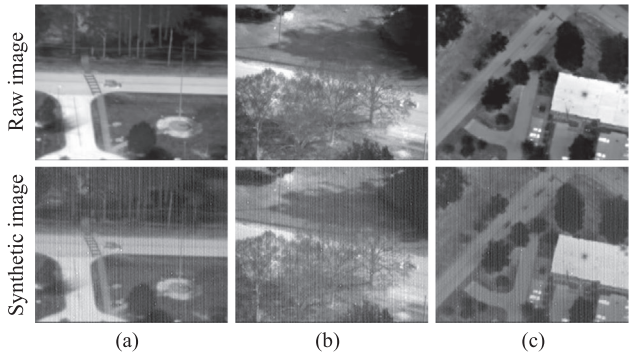

Fig. 8. Synthetic infrared images. (a) sequence 1 (b) sequence 2 (c) sequence 3.

of subband images $x_{j,k}^t$

Step 3: estimate the FPN variance of each subband by Eq. (14) and the FPN confidence by Eq. (15).

Step 4: estimate the FPN component $f_{j,k}^t$ of each subband $x_{j,k}^t$ by Eq. (10).

Step 5: subtract estimate the FPN component from each subband $x_{j,k}^t$ to calculate the estimated subban $\hat{y}_{j,k}^t$.

Step 6: implement the inverse Shearlet Transform to the processed subbands $\hat{y}_{j,k}^t$ to obtain the corrected infrared image.

Step 7: repeat the step 2 to step 7 until all infrared images have been corrected.

4. Experimental results and analysis

4.1. Experimental setting

The proposed method is called Shearlet Transform temporal high-pass (STTH) NUC in the following section. In the proposed method, the scale level of ST is 3 and each level has 10 orientations, the shape parameter of sigmoid function ε is set as 0.5.

Our experiments evaluate the proposed method and compare it with three typical THP-NUC methods from literatures as follows. (1) space low-pass and temporal high-pass (SLTH) NUC [15]. The mean filter size is set as 5. (2) bilateral filter based temporal high-pass (BFTH) NUC [16]. (3) motion region and high brightness region detection base (MDTH) NUC [17]. The experimental parameters of BFTH and MDTH are set as same as the reference paper. The test image is linearly mapped to the range 0 to 1 for comparability and the time constant of filter M is set as 20 for all the methods.

4.2. Results of real infrared sequences

In this section, three real infrared sequences obtained by a cooled infrared camera are utilized to evaluate the effectiveness of the proposed method. One of image in the original sequence is shown in Fig. 6 and correction results are shown in Fig. 7. As can be seen from original images, the stripe FPN influences the image quality seriously. Besides, the IRFPA is also affected by blind pixel (the pixels that have no response when the external thermal radiation changes). For these images, these white points are generated by blind pixel. The first sequence is

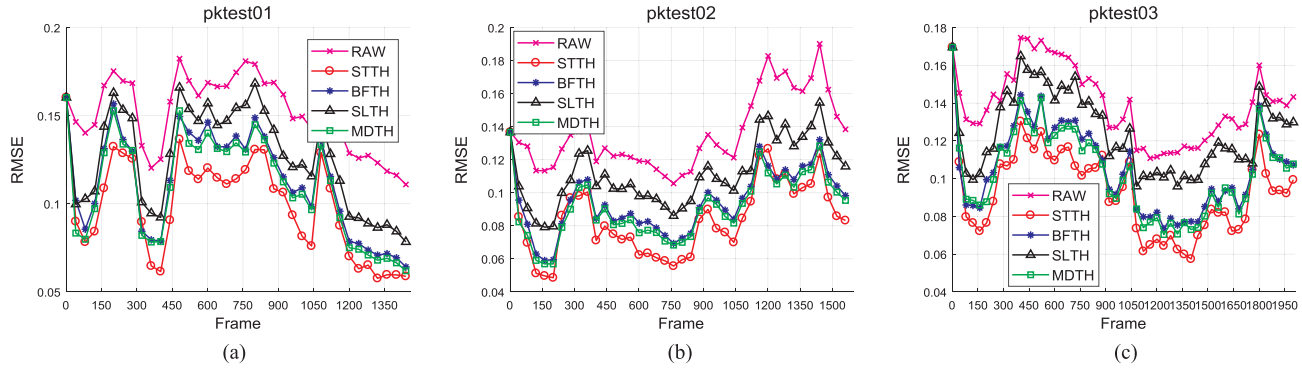

Fig. 9. The roughness curvess. (a) sequence PkTest01 (b) sequence PkTest02 (c) sequence PkTest03.

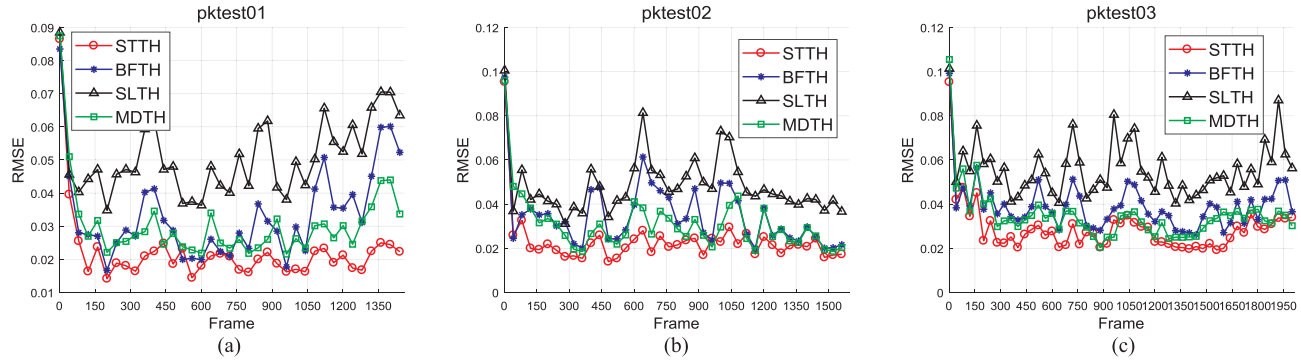

Fig. 10. The RMSE curvess. (a) sequence PkTest01 (b) sequence PkTest02 (c) sequence PkTest03.

Table 1
The average RMSE of sequences (The minimum is marked in bold).

Method	Sequence ($\times 10^{-1}$)		
	PkTest01	PkTest02	PkTest03
RAW	1.51	1.36	1.39
STTH	**0.98**	**0.84**	**0.93**
BFTH	1.12	0.94	1.05
SLTH	1.26	1.12	1.24
MDHD	1.09	0.90	1.03

Table 2
The average roughness of sequences (The minimum is marked in bold).

Method	Sequence ($\times 10^{-2}$)		
	PkTest01	PkTest02	PkTest03
STTH	**2.27**	**2.17**	**2.88**
BFTH	3.34	3.15	3.92
SLTH	5.16	4.78	5.59
MDHD	3.09	2.84	3.48

Table 3
The average time of different NUC methods.

Method	STTH	BFTH	SLTH	MDHD
Time per frame(s)	0.47	0.21	0.01	0.21

recorded by moving the camera steadily and the scene is static at the selected frame. In the way, the problem of image blurring can be evaluated. The second and the third sequences are recorded with complex situation. The camera perspective and people in the scene are moving with random direction. In this way, the problem of ghosting can be evaluated.

Correction results of SLTH are indicated in Fig. 7(b). This method utilizes the average filter to estimate the FPN and it is very difficult to separate the FPN completely, especially under the situation with serious FPN. Thus a lot of stripe pattern is remained in the corrected image.

There are slight FPN seen in the correction results of BFTH-NUC shown in Fig. 7(c). The bilateral filter is a good filter for image denoising because it utilizes the local similarity of the distance and gray value. However, in the heavy FPN region, this strategy cannot achieve good result because the FPN act as the same pattern in the local region, such as stripe pattern. Besides, the filter degree is always the same in different situation. If we separate more parts to the spatial high frequency, the FPN can be removed totally, but the details of image will be fuzzy. Otherwise, more FPN would remain. In all, this algorithm cannot decompose the image elaborately.

The correction results of MDHD are indicated in Fig. 7(d). This method first detect the motion between adjacent frames. Only in the situation with sufficient motion, the correction process is proceeded. This is a simple way to eliminate the image blurring in the static scene. However, it decreases the convergence speed of NUC. Then, the high brightness region is detected and the region with serious brightness variation has more contribution. The blind pixels are also high brightness region, thus this method cannot handle these pixel. Most of blind pixels can be seen from the corrected images.

The correction results of the proposed method are indicated in Fig. 7(b). The stripe FPN is mostly removed and the phenomenon of ghosting and image blurring don't occur. Thanks to the ST, most of FPN can be separated from the original image and be eliminated in the process of temporal high pass filter. Besides, the adaptively FPN confidence parameter is a useful strategy to control the filter degree. Most details in the raw image are retained. Obviously, the result of the proposed algorithm has the best visual effect in all sequences.

4.3. Results of synthetic infrared sequences

In this section, in order to objectively evaluate the proposed method, three public infrared sequences (PkTest01, PkTest02, PkTest03) with litter FPN form Vivid dataset [21] are selected. The synthetic infrared sequences are generated by adding the FPN on the original images and the simulated FPN is cropped from the real infrared image in Section 4.2. An example of the synthetic sequences is illustrated in Fig. 8. The first row is the raw images which are very clear and can be seen as the ground truth. The second raw is the example of the synthetic

Two objective indicators are utilized to evaluate the quality of the correction results. The roughness (ρ), can be utilized to evaluate the smooth degree of correction results which is defined as

$$\rho = \frac{\|h_1 * x_1\| + \|h_2 * x_1\|}{\|x_1\|} \tag{16}$$

where x is infrared image under analysis, $h_1 = [1, -1]$ is horizontal mask and $h_2 = {h_1}^{\mathrm{T}}$ is vertical mask. Operator * indicates the discrete convolution operation; $\|\|_1$ indicates L_1 norm.

Generally, the smaller value of roughness represents the better correction result. However, this also means the detail loss of the original image. Thus, the root-mean-square error (RMSE) is introduces to reflect the accuracy of correction result. This indicator calculate the difference between the corrected image and the real image which is defined as

$$RMSE = \sqrt{\frac{1}{m}\sum_{i=1}^{m}(y_i - x_i)^2} \tag{17}$$

where y is the corrected image and x is the real infrared image, and i is the i-th infrared pixel, m is the total number of pixel in the image. The roughness curves and RMSE curves of synthetic sequences are shown in Figs. 9 and 10 respectively.

As can be seen from Fig. 9, during the first 50 frames, the roughness curves drop rapidly. However, the simple mean filter cannot suppress the serious FPN. There always some stripe patterns left in corrected images. Thus, the roughness of STTH is larger than others after 50-th frames. Both the BFTH and the MDTH utilize bilateral filter to separate the FPN. The bilateral cannot utilize the structure information of the image. Thus, they cannot correct the non-uniformity totally. Thanks to the accurate FPN separation and adaptive filter degree, the proposed algorithm has better capability to remove the FPN, as it has smaller value of roughness.

From Fig. 10, it can be seen that compare to the other methods, RESE curves of the proposed algorithm are the smallest, which means corrected results are most accurate among these methods. Moreover, after one hundred frame, the curves of STTH have the least fluctuation, which means the proposed method has more steady convergence speed and can get more robust correction results.

The mean value of roughness and RMSE of each corrected sequence with four methods are shown in Tables 1 and 2. As can be seen from results, both the roughness and the RMSE obtained with the proposed method in this paper is the minimum compared with that of the other two algorithms.

Besides, the average time of different NUC method is listed in Table 3. These results are calculated in MATLAB (R2015a) on a computer of 4 GB RAM and Intel(R) Core(TM) i3-2120 CPU. As can be seen form results, the SLTH is the fastest method. BFTH and MDHD methods are nearly the same and the STTH is the slowest.

In summary, these above-mentioned results indicate that the proposed algorithm balances the correction result and the visual effect, and has better performance of non-uniform correction in the aspects of both objective evaluation and subjective visual. However, the proposed algorithm is relatively time-consuming, some parallel tools such as GPU and FPGA should be utilized to realize the real-time implementation in the practical application.

5. Conclusion

An improved temporal high pass NUC method is proposed in this paper. Through the Shearlet transform, the raw infrared image is decomposed into multiscale and multi-orientation subbands. Based on the variance of each subbands, different filter strategy is utilized to process each subband. In this way, the FPN can be removed more accurately and the proposed method also can adapt complex motion situation with less phenomenon of the ghosting and the image blurring.

However, because all subbands are needed to process by the temporal high pass filters, the proposed method has relatively larger computation complexity. Besides, the infrared image is also impacted by the spatial low-frequency FPN and each IRFPN has its unique pattern. There is not a certain assumption to cover all the possibility. Correcting the spatial low-frequency FPN and improve the real-time performance are our research key points in the future.

Acknowledgements

We would like to express our sincere appreciation to the anonymous reviewers for their insightful and valuable comments, which have greatly helped us in improving the quality of the paper. This work is partially supported by the 863 Program of China (2014AA8098089C), the National Natural Science Foundation of China (Nos. 61675160 and 61401343), the 111 Project (B17035), and Chinese Academy of Sciences (LSIT201503).

References

[1] A.F. Milton, F.R. Barone, M.R. Kruer, Influence of nonuniformity on infrared focal plane array performance, Opt. Eng. 24 (5) (1985) 855–862.
[2] H.X. Zhou, S.Q. Liu, R. Lai, D.B. Wang, Y.B. Cheng, Solution for the nonuniformity correction of infrared focal plane arrays, Appl. Optics 44 (15) (2005) 2928–2932.
[3] J.G. Harris, Y.M. Chiang, Nonuniformity correction of infrared image sequences using the constant-statistics constraint, IEEE Trans. Image Process. 8 (8) (1999) 1148–1151.
[4] S.E. Godoy, J.E. Pezoa, S.N. Torres, Noise-cancellation-based nonuniformity correction algorithm for infrared focal-plane arrays, Appl. Optics 47 (29) (2008) 5394–5399.
[5] D.A. Scribner, K.A. Sarkady, M.R. Kruer, J.T. Caulfield, J.D. Hunt, C. Herman, Adaptive nonuniformity correction for Infrared focal plane arrays using neural networks, Infrared Sens.: Detect, Electron. Signal Process. 1541 (1991) 100–109.
[6] R.C. Hardie, M.M. Hayat, E. Armstrong, B. Yasuda, Scene-based nonuniformity correction with video sequences and registration, Appl Optics 39 (8) (2000) 1241–1250.
[7] D.B. Zhou, D.J. Wang, L.J. Huo, R. Liu, P. Jia, Scene-based nonuniformity correction for airborne point target detection systems, Opt. Express 25 (13) (2017) 14210–14226.
[8] E. Vera, P. Meza, S. Torres, Total variation approach for adaptive nonuniformity correction in focal-plane arrays, Opt. Lett. 36 (2) (2011) 172–174.
[9] H. Yu, Z.-J. Zhang, C.-S. Wang, An improved retina-like nonuniformity correction for infrared focal-plane array, Infrared Phys. Technol. 73 (2015) 62–72.
[10] S.H. Rong, H.X. Zhou, H.L. Qin, R. Lai, K. Qian, Guided filter and adaptive learning rate based non-uniformity correction algorithm for infrared focal plane array, Infrared Phys. Technol. 76 (2016) 691–697.
[11] Z. Zhuang, H. Wang, A novel nonuniformity correction algorithm based on speeded up robust features extraction, Infrared Phys. Technol. 73 (2015) 281–285.
[12] S.H. Rong, H.X. Zhou, H.L. Qin, R. Lai, K. Qian, Nonuniformity correction for an infrared focal plane array based on diamond search block matching, J. Opt. Soc. Am. A 33 (5) (2016) 938–946.
[13] M. Maggioni, E. Sanchez-Monge, A. Foi, Joint removal of random and fixed-pattern noise through spatiotemporal video filtering, IEEE Trans. Image Process. 23 (10) (2014) 4282–4296.
[14] D.R. Pipa, E.A.B. da Silva, C.L. Pagliari, P.S.R. Diniz, Recursive algorithms for bias and gain nonuniformity correction in infrared videos, IEEE Trans. Image Process. 21 (12) (2012) 4758–4769.
[15] W.X. Qian, Q. Chen, G.H. Gu, Space low-pass and temporal high-pass nonuniformity correction algorithm, Opt. Rev. 17 (1) (2010) 24–29.
[16] C. Zuo, Q.A. Chen, G.H. Gu, W.X. Qian, New temporal high-pass filter nonuniformity correction based on bilateral filter, Opt. Rev. 18 (2) (2011) 197–202.
[17] Z.L. Li, T.S. Shen, S.L. Lou, Scene-based nonuniformity correction based on bilateral filter with reduced ghosting, Infrared Phys. Technol. 77 (2016) 360–365.
[18] G. Easley, D. Labate, W.Q. Lim, Sparse directional image representations using the discrete shearlet transform, Appl. Comput. Harmon. A. 25 (1) (2008) 25–46.
[19] H.Y. Yang, X.Y. Wang, P.P. Niu, Y.C. Liu, Image denoising using nonsubsampled shearlet transform and twin support vector machines, Neural Networks 57 (2014) 152–165.
[20] S.G. Chang, B. Yu, M. Vetterli, Adaptive wavelet thresholding for image denoising and compression, IEEE T. Image Process. 9 (9) (2000) 1532–1546.
[21] http://vision.cse.psu.edu/data/vividEval/datasets/datasets.html.